DOI: 10.1002/ejic.201100411

Interfacial Electron Transfer Dynamics of Two Newly Synthesized Catecholate Bound Ru^{II} Polypyridyl-Based Sensitizers on TiO_2 Nanoparticle Surface – A Femtosecond Pump Probe Spectroscopic Study

Tanmay Banerjee,[b] Sachin Rawalekar,[a] Amitava Das,*[b] and Hirendra N. Ghosh*[a]

Keywords: Ruthenium / Nanoparticles / Electron transfer / Electron-donating group / Time-resolved spectroscopy

Two new catecholate-bound Ru^{II}–polypyridine based sensitizers, (2,2′-bipyridine){ethyl 3-(4-hydroxyphenyl)-2-[(4′-methyl-2,2′-bipyridinyl-4-carbonyl)amino]propionate}{4-[2-(4′-methyl-2,2′-bipyridinyl-4-yl)vinyl]benzene-1,2-diol)}ruthenium(II) hexafluorophosphate (**5**) and [(2,2′-bipyridine)-(4-2,2′-bipyridinyl-4-yl-phenol)-(4-{2-(4′-methyl-2,2′-bipyridinyl-4-yl)vinyl}benzene-1,2-diol)]ruthenium(II) hexafluorophosphate (**6**) with secondary electron-donating groups (tyrosine and phenol, respectively) were synthesized and characterized. Steady-state optical absorption and emission studies confirm strong coupling between the sensitizers and TiO_2 nanoparticles. Femtosecond visible transient absorption spectroscopy has been employed to study interfacial electron transfer (IET) dynamics in the dye–nanoparticle systems to explore the influence of the secondary electron-donating groups on IET dynamics. Electron injection into the conduction band of nanoparticulate TiO_2 has been confirmed by detection of the conduction band electrons in TiO_2 ($[e^-]_{TiO2}^{CB}$) and radical cation of the adsorbed dye (D^{+}) in real time monitored by transient absorption spectroscopy. A single exponential and pulse-width limited (< 100 fs) electron injection has been observed. Back electron transfer (BET) dynamics have been studied by monitoring the decay kinetics of the injected electron in the conduction band of TiO_2 and by the recovery of the ground state bleach. BET dynamics in dye–TiO_2 systems for complexes **5** and **6** have been compared with those of [bis(2,2′-bpy)-(4-{2-(4′-methyl-2,2′-bipyridinyl-4-yl)vinyl}benzene-1,2-diol)]ruthenium(II) hexafluorophosphate (**7**), which does not have a secondary electron-donating group.

Introduction

Research in the area of nanocrystalline dye-sensitized solar cells (DSSC) has attracted considerable interest owing to their potential applications as cost-effective alternatives to current p–n junction photovoltaic devices.[1–4] The studies in this area have intensified over the past decade with an aim to improve the overall conversion efficiency (η) from 10.4%, a value achieved by Grätzel and coworkers[2] in N3-sensitized TiO_2 DSSC.[5–10] Over the years efficient dye-sensitized solar cells based on Ru^{II}–polypyridine complexes attached to nanocrystalline TiO_2 have been developed.[4,11–18] Ru^{II}–polypyridine complexes have been the choice because of their prominent visible absorption bands, long-lived excited states and their distinctive photochemical stability.

One of the major factors controlling the overall light-to-current conversion yield in such light-harvesting devices is the effective charge separation at the sensitizer–semiconductor interface, and a long lived charge separated state is imperative in order to obtain a good photocurrent response. Longer lived charge separated states may be achieved by making the positive charge move away from the photo-oxidized sensitizer core, which is possible by covalently attaching an electron donor to the sensitizer. By connecting phenothiazine or triarylamine to Ru^{II}–polypyridine-based complexes, long lived charge separation has been obtained.[19–29] Much work has been carried out on systems where a secondary redox couple based on phenol has been used to rereduce the Ru^{III} created by excited state electron transfer to nanoparticulate TiO_2 analogous to electron transfer from Tyr_z to P 680 in photosystem II.[30,31] However, most of this work has been carried out with sensitizers based on carboxylate anchoring groups, which have certain disadvantages. Due to the low pK_a of carboxylates ($pK_a \approx 3.5$)[32,33] there remains a possibility of slow desorption of the sensitizer dye molecules from the surface of semiconductor in the presence of water. Furthermore, dyes with carboxylate anchoring groups generally show biphasic electron injection.[17,34] Our previous reports show that ruthenium–polypyridyl-based sensitizer dyes with catecholate anchoring groups inject electrons into TiO_2 single exponentially and within instrumental pulse width (< 100 fs)[35–37] in contrast to dyes with carboxylate anchoring groups. In addition, catecholates have pK_a values greater than 9.6 and,

[a] Radiation and Photo Chemistry Division, Bhabha Atomic Research Center,
Mumbai, India
Fax: +91-22-25505151
E-mail: hnghosh@barc.gov.in
[b] Analytical Science Discipline, Central Salt and Marine Chemicals Research Institute,
Bhavnagar, Gujarat, India
Fax: +91-278-2567562
E-mail: amitava@csmcri.org

even at higher pH, the possibility of the dye molecules becoming desorbed from the surface of the semiconductor is excluded. Moreover, studies concerning the effects of the electron donor have been limited to longer time domains (micro- and millisecond) when a good fraction of charge separated species have already undergone a charge recombination reaction. As a result it is difficult to understand the effect of the secondary electron-donating group in IET dynamics. To understand the mechanism and the effect, it is very important to study IET dynamics on the ultrafast timescale.

With these aspects in mind we have synthesized two new Ru^{II}–polypyridyl-based sensitizer molecules, **5** and **6** (Scheme 1), with different electron-donating abilities of the secondary groups (tyrosine and phenol, respectively) and a catecholate anchoring group to bind to TiO_2 nanoparticles. Steady state optical absorption and emission studies confirm strong binding of the sensitizer molecules to TiO_2. To understand the effect of secondary electron-donating groups on the ultrafast timescale, we have studied the IET dynamics in **5**- and **6**-sensitized TiO_2 nanoparticles using femtosecond transient absorption spectroscopy and the results have been compared with our previous results for **7**-sensitized TiO_2 nanoparticles.[37]

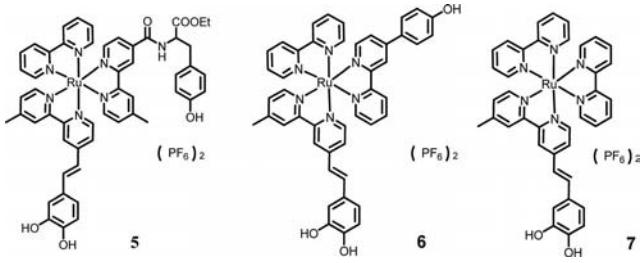

Scheme 1. Molecular structures of **5**, **6** and **7**.

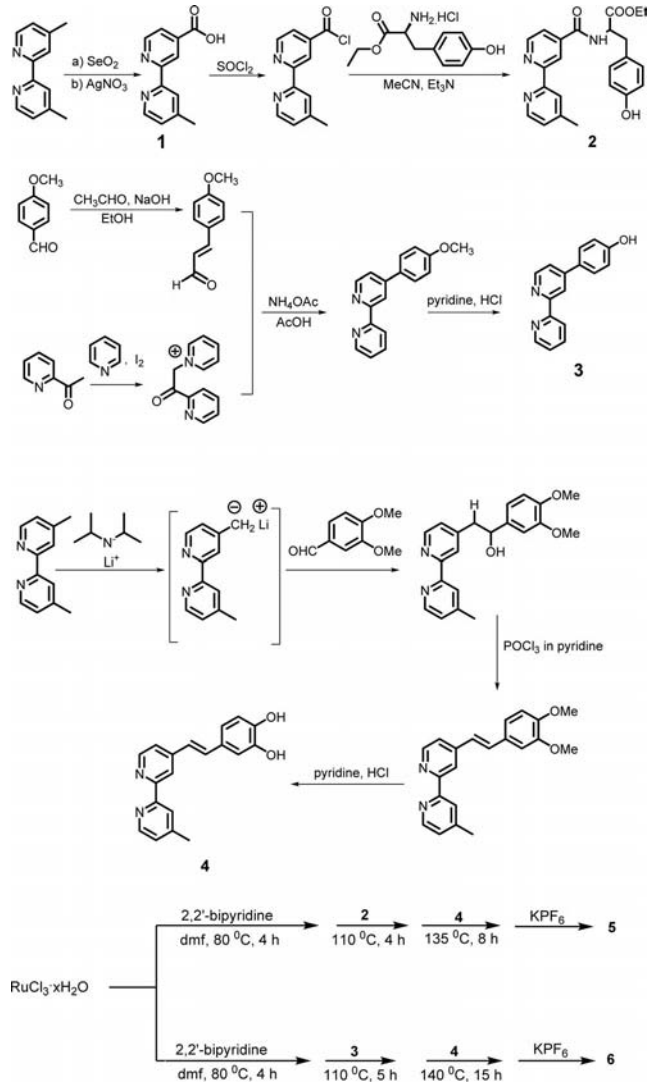

Scheme 2. Synthetic route for the preparation of **5** and **6**.

Results and Discussion

Synthesis

The synthetic methodology adopted for the synthesis of the bipyridine-based ligands and complexes are outlined in Scheme 2. 4-(2,2′-Bipyridinyl-4-yl)phenol and 4-[2-(4′-methyl-2,2′-bipyridinyl-4-yl)vinyl]benzene-1,2-diol were synthesized as per previous reports and the analytical data matched well with that of the reported compounds. Compound **1** was prepared by a selenium dioxide oxidation of 4,4′-dimethyl-2,2′-bipyridine followed by further oxidation with silver nitrate. The excess silver nitrate was precipitated as silver oxide and was removed by filtration. Adjusting the pH of the aqueous extract to about 3.5 precipitated the carboxylic acids formed. A continuous Soxhlet extraction of this mixture over seven days gave pure **1**.

Compound **1** was converted into its acyl chloride and this was reacted with L-tyrosine ethyl ester hydrochloride in acetonitrile in presence of triethylamine. Purification by column chromatography yielded pure **2**. Complex **5** was prepared in a one pot reaction where $RuCl_3 \cdot xH_2O$ was allowed to react successively with molar equivalents of 2,2′-bipyridine, **2** and **4** at different time intervals at progressively higher temperatures. After evaporation of the solvent, anion exchange was carried out in acetonitrile by stirring in the presence of excess potassium hexafluorophosphate. Acetonitrile was used because the product was only partially soluble in water. The crude product was purified by column chromatography and was further purified by vapour diffusion method of recrystallization. Complex **6** was prepared following a similar methodology. The addition of 4-[2-(4′-methyl-2,2′-bipyridinyl-4-yl)vinyl]benzene-1,2-diol (**4**) however required a longer time and a higher temperature compared to that in the synthesis of complex **5**. The purity of the complexes was checked by different analytical and spectroscopic methods and the analytical data matched well with those of the expected formulations.

Spectroscopic Properties – UV/Vis Absorption and Photoluminescence Measurements

Figure 1 shows the optical absorption spectra of **5** and **6** in acetonitrile. The spectrum of **7** is included for comparison.[37] The low energy broad absorption band for **5** at 456 nm and that of **6** at 456 nm along with a shoulder at 433 nm arise due to overlapping metal-to-ligand charge transfer (MLCT) based $d_{Ru}{}^{II} \rightarrow \pi^*_{2,2'-bpy}$, $d_{Ru}{}^{II} \rightarrow \pi^*_{bpy-cat}$ and $d_{Ru}{}^{II} \rightarrow \pi^*_{bpy-tyr}$ or $d_{Ru}{}^{II} \rightarrow \pi^*_{bpy-phenol}$ transitions. The absorption of tyrosine ($\lambda_{max} \approx 274$ nm, $\varepsilon = 1405$)[38] in **5** and that for phenol in **6** (λ_{max} at ca. 270 nm, $\varepsilon = 2340$)[39] are masked due to strong intra- and/or interligand π–π* transitions at 288 nm ($\varepsilon \approx 10^5$),[40,41] and the band at 245 nm along with the shoulder at 253 nm are assigned to higher energy MLCT d–π* transitions.[41] The absorption bands at 354 and 322 nm for **5** and **6**, respectively, can be attributed to interligand charge transfer transitions from π_{bpy} to $\pi^*_{bpy-tyr}$ and from π_{bpy} to $\pi^*_{bpy-phenol}$.[41] The relative shift of 32 nm for **6** compared to **5** is due to the higher donating ability of phenol (E^{ox} = 0.98 V) compared to tyrosine (E^{ox} = 1.03 V) (see below for electrochemical data).

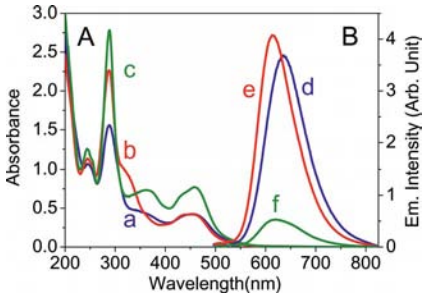

Figure 1. A: Absorption spectra of (a) **5**, (b) **6** and (c) **7** in acetonitrile ($c = 3 \times 10^{-5}$ M); B: Emission spectra of (d) **5**, (e) **6** and (f) **7** in acetonitrile. Emisson spectra were recorded for identical absorbances of the three complexes at an excitation wavelength of 457 nm.

Steady state emission spectra of **5**, **6** and **7** in acetonitrile were also recorded and these are shown in part B of Figure 1. In this study our main aim is to find the effect of electron-donating groups in Ru complex-sensitized TiO_2 nanoparticles after exciting the MLCT band. Therefore, we have carried out steady state emission studies of **5** and **6** after excitation at 456 nm. Figure 1 (B) shows that **5** emits with λ_{max} at 635 nm, and **6** emits at 614 nm. The blueshift observed in the emission spectrum of **6** compared to that of **5** is due to the presence of the phenol moiety, which acts as a better donor than tyrosine and raises the π^*_{bpy} lowest unoccupied molecular orbital level. Interestingly, although we observe the emission intensity of **5** and **6** to be similar, the emission intensity of **7** (Figure 1, f) is much lower than that of **5** and **6** in spite of the absence of an electron-donating group. This might be due to the fact that the excited state potential surface of **7** is dominated by the bpy–catechol ligand where the de-excitation process is very fast due to H-bond interactions between the solvent and the catechol moiety. However, in case of **5** and **6**, the excited state potential surface also contains a contribution from their electron-donating ligands and nonradiative transitions are less active compared to **7**.

Electrochemical Studies

Cyclic voltammograms of **5** and **6** in acetonitrile were very similar in nature (Figure 2). The $Ru^{II/III}$ redox potential for **5** was 1.35 V and that of **6** was 1.30 V in degassed acetonitrile. Both tyrosine and phenol show irreversible oxidation peaks at 1.03 and 0.98 V in **5** and **6**, respectively. The irreversible nature of the oxidation peak has been previously reported for phenols, and is because the oxidized species have lifetimes shorter than the timescale of the instrument.[42] The potential values quoted henceforth for these electron-donating phenolic groups are therefore the oxidation potentials and those for the metal centre are the redox potentials.

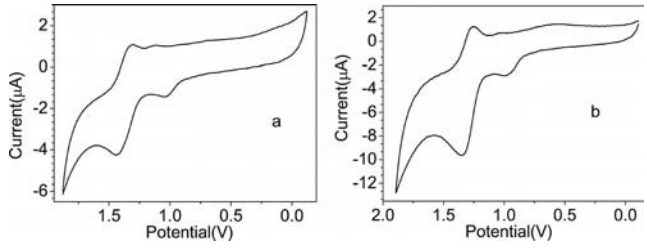

Figure 2. Cyclic voltammograms of (a) **5** and (b) **6** in acetonitrile. A saturated calomel electrode (SCE) was used as the reference electrode. The scan rate for both scans was 100 mV/s.

In order to comprehend the feasibility of electron injection into the conduction band of the semiconductor nanoparticles it becomes necessary to calculate the redox potential of the excited state of the dye. The E_{0-0} transition energy was calculated to be 2.21 and 2.24 eV for **5** and **6**, respectively, from the intersection points of the excitation and emission spectra in acetonitrile. The excited state potentials $E(S+/S^*)$[43,44] were thus calculated to be –0.86 and –0.94 V for **5** and **6**, respectively, following the equation $[E(S+/S^*)] = [E(S+/S)] - E_{0-0}$. The excited state potentials being above the conduction band level, electron injection from the excited state of the sensitizers into the conduction band of TiO_2 is feasible. As evident from the cyclic voltammograms, the oxidation potential of the tyrosine and phenolic moieties in **5** and **6** are lower than the oxidation potential of the ruthenium centre. Therefore, electron transfer from tyrosine or phenol to the Ru^{II} centre is thermodynamically possible.

Dye Binding with TiO_2 Nanoparticles

The aim of this investigation is to study IET on semiconductor surfaces, therefore it is very important to study the binding properties of the dye and nanoparticulate semiconductor systems. The nature of the binding between a sensitizer and a semiconductor is known to influence the excited

state properties and IET behaviour.[4] Strong binding serves to anchor the sensitizer in place and control interfacial electronic coupling. This is also known to influence the redox potentials of the sensitizers and the semiconductor nanoparticles. We have observed that Ru^{II}– and Os^{II}–polypyridyl complexes with pendant catecholate moiety bind strongly to TiO_2 nanoparticles.[35–37,45,46] Figure 3 shows the optical absorption and emission spectra of **5** and **6** in aqueous solution in the presence and absence of TiO_2 nanoparticles. The spectral features observed in water are very similar to those in acetonitrile (Figure 1). The absorption spectra show a prominent increase and broadening, along with a slight red-shift, of the MLCT band at 456 nm in the presence of TiO_2 nanoparticles for both complexes, which can be explained by a strong interaction of the sensitizer molecules with TiO_2 nanoparticles through the formation of a five-membered ring.[47,48] This observation is in accordance with results reported earlier where we have shown that dyes bound to the TiO_2 surface through catecholate anchoring groups interact very strongly.[35,36,45,46,49–52]

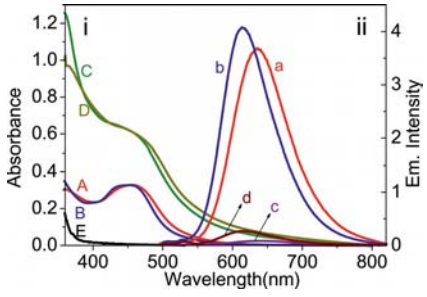

Figure 3. i) Absorption spectra of A: **5**, B: **6**, C: **5** in the presence of TiO_2 nanoparticles, D: **6** in the presence of TiO_2 nanoparticles and E: TiO_2 nanoparticles; ii) emission spectra of a: **5**, b: **6**, c: **5** in the presence of TiO_2 nanoparticles and d: **6** in the presence of TiO_2 nanoparticles. Dye concentration for all UV measurements is 2.5×10^{-5} M, and 3×10^{-5} M for the fluorescence measurements. TiO_2 concentration is 20 g/L for all measurements.

To confirm the formation of the complex, we have constructed a Benesi–Hildebrand plot for **5** and **6** by recording the optical absorption spectrum of the complexes with increasing TiO_2 concentrations. From the Benesi–Hildebrand plot, equilibrium constants of 5.33×10^3 and 4.28×10^3 M^{-1} were determined for **5**–TiO_2 and **6**–TiO_2, respectively. Molar extinction coefficients of 1.04×10^4 $M^{-1}cm^{-1}$ were determined for both **5**–TiO_2 and **6**–TiO_2. The strong interaction of the sensitizers with the semiconductor nanoparticles is further supported by the fact that the luminescence spectra of both the complexes are quenched considerably in the presence of TiO_2 nanoparticles due to electron injection (Figure 3). Thus, steady state studies confirm strong binding of the sensitizer molecules with the nanoparticles and permit further studies into their effectiveness as efficient sensitizers and the possible effects of the electron-donating groups attached.

Excited State Dynamics of the Free Complexes in Acetonitrile

In order to develop a comprehensive understanding of the dynamics of electron injection into the semiconductor nanoparticles, it is essential to study the excited state dynamics of the photoinduced processes associated with the free sensitizer molecules. We have carried out femtosecond transient absorption studies (in the visible and near IR region) of **5** and **6** in acetonitrile. Figures 4 and 5 show the transient absorption spectra of **5** and **6** in acetonitrile, respectively.

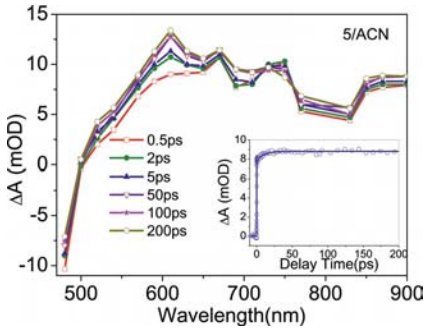

Figure 4. Transient absorption spectra of **5** in acetonitrile at different delay times following excitation at 400 nm. Inset: kinetic trace of the excited triplet state (^{3}MLCT) of **5** at 650 nm in acetonitrile after excitation at 400 nm.

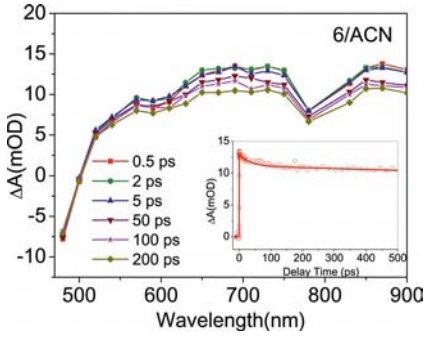

Figure 5. Transient absorption spectra of **6** in acetonitrile at different delay times following excitation at 400 nm. Inset: kinetic trace of the excited triplet state (^{3}MLCT) of **6** at 650 nm in water after excitation at 400 nm.

Both spectra show two broad absorption features, one ranging from 510–780 nm and the other in the near IR region ranging from 830–1000 nm along with a bleach before 500 nm due to ground state MLCT absorption. These transient absorption bands are assigned to excited triplet state absorption,[35–37,46] because intersystem crossing in Ru^{II}–polypyridyl complexes is known to be very fast and is completed in 15 ± 10 fs.[53] Thus, the singlet to triplet conversion is expected to have occurred within the pulse width of the instrument (< 100fs). We monitored excited state dynamics of **5** and **6** by monitoring the kinetics at 650 nm, shown inset in Figure 4 and Figure 5, respectively.

The kinetic trace for **5** at 650 nm was found to have biexponential growth with time constants of < 100 fs (85%) and 10 ps (15%). The first growth component is pulse width

limited (< 100 fs) and can be attributed to the formation of a singlet and/or triplet state. The second growth component can be attributed to a vibrational relaxation of the ^{3}MLCT state.[37,54–56] It has also been observed that the kinetic trace does not decay on the 1 ns timescale. On the other hand, the kinetic decay trace of **6** monitored at 650 nm shows single exponential growth (< 100 fs) followed by biexponential decay with time constants of 30 ps (15.4%) and > 1 ns (84.6%). As reported previously, the lifetimes of the triplet MLCT state of Ru^{II}–polypyridyl complexes are > 100 ns,[57] so we can safely attribute these long components in both complexes to excited triplet states. It is interesting to see that **6** (Figure 5, inset) has an extra decay time constant of 30 ps in addition to the > 1 ns component compared to **5**, which has only one decay component of > 1 ns. We have previously carried out ultrafast excited spectroscopic studies on a series of ruthenium complexes[35,37,46] and observed only one long time decay component (> 1 ns), except for $Ru(CN)_4$(bpy–cat),[2–36] which has an extra decay component of 10 ps. This component was thought to be due to an extra decay channel associated with the excited states. The cyano groups might form H-bonds with the surrounding solvent molecules and so the excited state energy could relax to the solvent through the H-bonds. In a similar way, the hydroxy group of the bpy–phenol moiety in **6** can form H-bonds with the solvent molecules and the excited state could relax resulting in the 30 ps decay component. The phenolic hydroxy group is in direct conjugation with the chromophore centre in **6**, unlike that in **5**, which is linked by a nonconjugated amide spacer. This could be the reason why the decay component is absent in **5**.

Transient Absorption Measurements of 5 and 6 on a TiO_2 Surface

In steady state emission studies we have observed that the photoluminescece intensity of both **5** and **6** was drastically reduced in the presence of TiO_2 nanoparticles (Figure 3), which confirmed IET from the sensitizers to TiO_2. To probe the ET dynamics and the effect of the electron-donating groups on a shorter timescale, we carried out femtosecond transient absorption measurements on the dye–TiO_2 systems following excitation with a laser source of 400 nm.

Figures 6 and 7 show the transient absorption spectra of **5**–TiO_2 and **6**–TiO_2, respectively. Both spectra show two broad absorption bands, one ranging from 540–750 nm and the other in the region of 800–1000 nm. The first absorption feature can be assigned to the formation of the radical cation ($\mathbf{5}^{\cdot+}$ or $\mathbf{6}^{\cdot+}$) based on our previous results.[35,37,46] The lower energy absorption band in the 800–1000 nm region is assigned to electrons in the conduction band of the TiO_2 nanoparticles. This assignment is corroborated by the detection of electrons in the conduction band by visible,[58,59,60] near IR[61] and mid IR[62,63] absorption. The kinetic decay trace of radical cations for both **5** and **6** are shown inset in Figures 6 and 7, respectively.

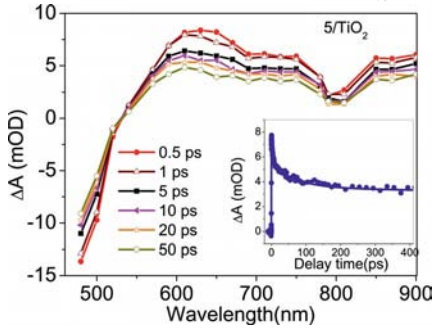

Figure 6. Transient absorption spectra of **5**–TiO_2 in water at different time delays after excitation at 400 nm. Typical concentration for **5** was ca. 200 μM and about 20 g/L for TiO_2 nanoparticles. Inset: kinetic trace of the radical cation of **5** ($\mathbf{5}^{\cdot+}$) at 590 nm.

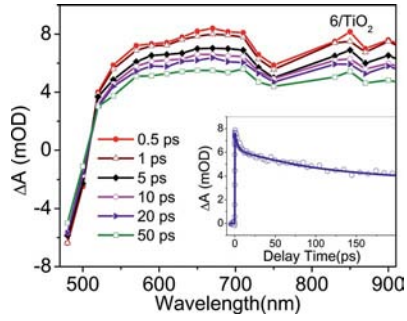

Figure 7. Transient absorption spectra of **6**–TiO_2 in water at different time delays after excitation at 400 nm. Typical concentration for **6** was ca. 200 μM and ca. 20 g/L for TiO_2 nanoparticles. Inset: kinetic trace of the radical cation of **6** ($\mathbf{6}^{\cdot+}$) at 610 nm.

The electron injection time can be predicted by monitoring the time of appearance of the electron signal. It was found to be pulse width limited (< 100 fs) and single exponential at all the wavelengths monitored and for both compounds. The electron is injected in majority from the nonthermalized states and not from the thermalized states, confirmed by the fact that no associated growth for either the radical cation signal or the electron signal was observed and that the kinetic traces decay with almost similar time constants from 540–900 nm. Had there been injection from the thermalized triplet states, we would have observed a growth of the radical cation signal in the early timescale along with a decay of the triplet state.[64]

In addition, our previous studies confirm that the transients obtained at different wavelengths are due to the charge separated species and that any contribution due to excited states is negligible.[35,36,46] The nonthermalized excited states involved in IET are presumably both the hot singlet and triplet states because the ISC process is known to be very fast in Ru^{II}–polypyridyl complexes and this competes with the electron injection into TiO_2. Complexes **5** and **6** are anchored to the TiO_2 surface through the catecholate functionality resulting in very strong electronic coupling, which is responsible for electron injection from the nonthermalized states, hence a single exponential and ultrafast electron injection. The main aim of this investigation is to monitor the effect of the electron-donating centre on

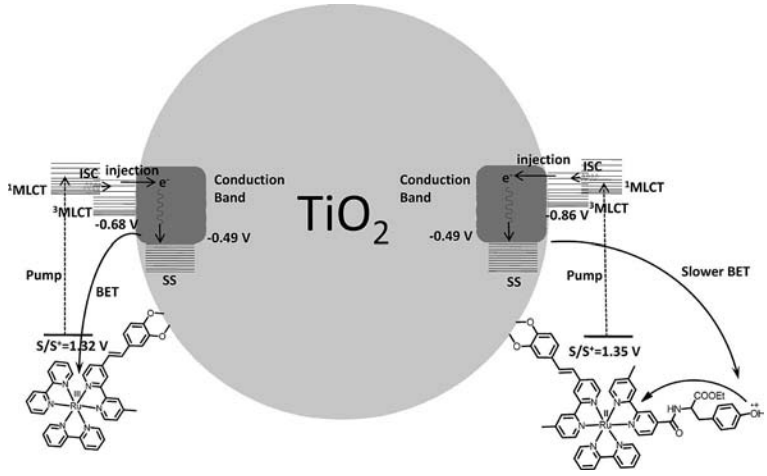

Scheme 3. Schematic representation of IET in **5**–TiO_2 and **7**–TiO_2. The effect of a secondary electron-donating group in the IET dynamics of **5**–TiO_2 has been demonstrated.

ET dynamics. Provided that the charge separation at the dye–semiconductor interface is maintained efficiently, the dye-sensitized solar cell can be made to work resourcefully. Charge recombination, i.e. BET dynamics, therefore becomes necessary to be studied as it is one of the major pathways for loss of the effective electron concentration in the conduction band. The injected electron has to escape from the reaction distance of recombination and reach the bulk of the electrode by downhill migration for it to contribute to the photocurrent response of the cell.[65] The dynamics of the BET process can be determined by monitoring the decay of either the conduction band electrons or the radical cation or by monitoring the recovery of the ground state bleach. Figure 8 (a and b) shows the bleach recovery kinetics of **5**–TiO_2 and **6**–TiO_2, respectively. In our earlier reports we discussed IET dynamics in **7**–TiO_2 where no electron-donating moiety was present (Scheme 3). In order to find the effect of the electron-donating groups, it is important to compare the BET dynamics of all the systems, (**5**-, **6**- and **7**-sensitized TiO_2 nanoparticles). We compare the bleach recovery kinetics for these three systems in Figure 8.

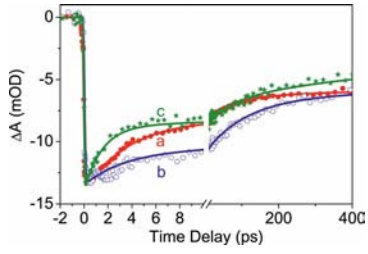

Figure 8. Bleach recovery kinetics at 480 nm in a) **5**–TiO_2, b) **6**–TiO_2 and c) **7**–TiO_2 system after excitation at 400 nm.

The kinetic traces of **5**–TiO_2 (Figure 8, a) and **6**–TiO_2 (Figure 8, b) can be fitted multiexponentially with time constants τ_1 = 2.7 ps (39.5%), τ_2 = 70 ps (16%) and $\tau_3 > 1$ ns (44.5%) and τ_1 = 3.3 ps (19%), τ_2 = 110 ps (32%) and $\tau_3 >$ 1 ns (49%), respectively. We have already reported the bleach recovery kinetics for **7**–TiO_2 fitted with time constants τ_1 = 1.5 ps (37.6%), τ_2 = 70 ps (19.4%), $\tau_3 > 1$ ns (43%) (Figure 8, c).

It is interesting to see that the bleach recovery kinetics is slowest for **6**–TiO_2. We have also monitored injected electron in the conduction band at 900 nm to compare the BET dynamics (Figure 9).

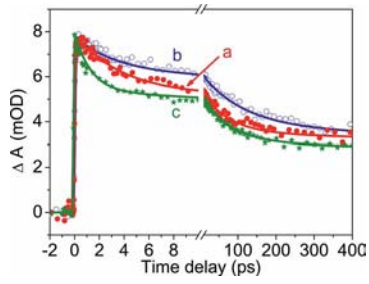

Figure 9. Transient decay kinetics of injected electron at 900 nm in a) **5**–TiO_2, b) **6**–TiO_2 and c) **7**–TiO_2 after excitation at 400 nm.

The kinetic traces of the injected electron in **5**–TiO_2 (Figure 9, a) and **6**–TiO_2 (Figure 9, b) can be fitted multiexponentially with time constants τ_1 = 3.5 ps (28%), τ_2 = 70 ps (28%) and $\tau_3 > 1$ ns (44%) and τ_1 = 3.3 ps (25.8%), τ_2 = 110 ps (29%) and $\tau_3 > 1$ ns (45.2%), respectively. For **7**–TiO_2 (Figure 9, c) kinetics at 900 nm[37] can be fitted with time constants τ_1 = 1.5 ps (34.8%), τ_2 = 70 ps (26.8%) and $\tau_3 > 1$ ns (38.4%). As is evident from the above time constants, the BET was found to be faster in these systems than that of dyes with carboxylate anchoring groups.[34,66] Stronger binding of the catecholate functionality is responsible for the fast BET in our systems.

Effect of Electron-donating Group in the IET Reaction

A good deal of research has been devoted to searching for ways to slow the charge recombination process between the photo-oxidized dye and the conduction band electrons in dye-sensitized TiO_2 nanoparticles. While it is possible to position the sensitizer core away from the nanoparticle sur-

face, a fast electron injection rate has to be compromised at the expense of slow charge recombination.[67,68] In another approach, people have tried introducing an additional electron donor so that the initial electron injection process is not affected. Several molecular dyads have been studied in this context.[19–21,23–29,69,70] Phenolic donor groups have been explored as an electron-donating functionality, in particular by Sundstrom et al.[30,31,71] Most of these studies have been carried out on the nano- and microsecond timescales. To understand the influence of the electron-donating moiety it is important to study and compare the ET dynamics for **5**, **6** and **7** on the ultrafast timescale. In this report, the electron transfer processes were initiated following a laser pulse of 400 nm, which populated the MLCT states and from which electrons are injected into the conduction band of TiO_2. Immediately after electron injection, a hole will be localized in the electron-donating groups (tyrosine and phenol) and as a result there will be an increase in spatial charge separation because the electron will be localized in TiO_2, and we expect that the BET dynamics will be slower.

We have shown the bleach recovery kinetics in Figure 8 for different systems, and it is clear that the charge recombination reaction is fastest in **7**–TiO_2 (where **7** does not have a secondary electron-donating group). We have also observed a similar trend as we have monitored the kinetic decay trace for the injected electron (Figure 9). From Figures 8 and 9 it is clear that the electron-donating groups play a major role in charge recombination reactions in dye–TiO_2 nanoparticle systems. Phenol is a better electron donor than tyrosine (as observed in electrochemical studies) and so, in the early timescale, the bleach recovery of **6**–TiO_2 is the slowest, followed by that of **5**–TiO_2, and the recovery of **7**–TiO_2 is the fastest. To confirm that the electron-donating group is indeed taking part in the electron transfer dynamics, it is important to monitor the oxidized donor moiety (tyrosyl and phenoxy radical cations in **5** and **6**, respectively) in the transient spectra. However, these radicals absorb below 450 nm in the transient spectra,[71,72] which is beyond the detection range of our femtosecond transient spectrometer (450–1000 nm). To reconfirm the influence of the electron-donating centers on the ET dynamics, we have determined the free energy of the respective reactions in our systems. Different BET rates for **5**, **6** and **7** can be explained by Marcus semiclassical electron transfer theory.[73] According to this theory, the BET rate constant (k_{BET}) is expressed as

$$k_{BET} = \left(\frac{2\pi}{\hbar}\right)[H_{AB}]^2 \frac{1}{\sqrt{4\pi\Lambda kT}} \exp\left\{-\frac{(\Delta G^0 + \Lambda)^2}{4\Lambda kT}\right\}$$

where H_{AB} is the coupling element, Λ is the reorganization energy and ΔG^0 is the overall free energy of the reaction. We can safely assume that the electronic coupling in the dye–nanoparticle systems is nearly the same as for **5**–TiO_2, **6**–TiO_2 and **7**–TiO_2 systems. The reorganization energy can also be assumed to be similar considering that all of the studies have been performed under identical conditions. Therefore, the BET rate for these systems will depend on the overall free energy of the reaction, provided that the effect of electron-donating group is absent. $\Delta G^0 = E_C - E_{S/S}^+$, where E_C (–0.49 V)[74] is the potential of the electrons in the conduction band of the semiconductor and $E_{S/S}^+$ is the redox potential of the dye. Using this equation the ($-\Delta G^0$) values for **5**–TiO_2, **6**–TiO_2 and **7**–TiO_2 were calculated to be 1.84 eV, 1.79 eV and 1.81 eV, respectively. Interestingly, the free energy of reaction ($-\Delta G^0$) is very similar for all three systems, although we observe very different ET dynamics. It has been demonstrated previously that the BET reaction in dye–TiO_2 systems falls into the Marcus inverted regime.[75–77] This means that as we increase the free energy of reaction ($-\Delta G^0$), the rate of reaction will decrease. In this study, if there was no effect of the electron-donating groups on the ET dynamics then we would have seen the fastest ET dynamics in **6**–TiO_2 as the free energy of the reaction ($-\Delta G^0$) is the lowest (1.79 eV). Therefore, we have clearly demonstrated the effect of the electron-donating groups on the ET dynamics. Based on our data and observations, Scheme 3 is proposed for photoinduced electron transfer processes for **5**–TiO_2 and **6**–TiO_2

After light excitation of the ruthenium chromophore, electron injection occurs from the MLCT excited state to TiO_2, producing the charge-separated state of Ru^{III} and electrons in the conduction band of TiO_2. The hole may now become localized in the secondary electron-donating groups and thus coupling between the electron in the conduction band and the hole in the sensitizer gets reduced. This might be responsible for the slow BET observed for **5**–TiO_2 and **6**–TiO_2 in the early timescale. It would have been best, had we been able to determine the rate of electron transfer from tyrosine or phenol to Ru^{III} by monitoring the respective oxidized radicals (tyrosyl and phenoxy) in the femtosecond transient absorption spectrum. We are developing new Ru^{II}–polypyridyl-based sensitizer dyes with covalently attached electron-donating groups such that the oxidized donor group can be monitored directly in the visible region (above 450 nm) so that the ET rate constants can be determined without ambiguity.

Conclusions

Two new Ru^{II}–polypyridyl complexes **5** and **6**, with pendant catecholate functionality and tyrosine or phenol as electron-donating groups, have been synthesized and characterized. The catecholate functionality allows strong coupling of these sensitizer molecules with nanoparticulate TiO_2. We have investigated IET dynamics in **5**–TiO_2 and **6**–TiO_2 using ultrafast transient absorption spectroscopy. On excitation with 400 nm laser pulse, a transient absorption band for the dye radical cation ($D^{\cdot+}$) and a broad absorption band for the conduction band electrons are observed. Electron injection was found to be single exponential and pulse width limited (< 100 fs) indicating electron injection from a nonthermalized singlet state (^{1}MLCT), and/or triplet state (^{3}MLCT). BET dynamics were studied by monitoring the decay kinetics of the injected electron in the conduc-

tion band of TiO_2 and by the recovery of the ground state bleach. BET dynamics for **5** and **6** were compared with that of previously reported **7**. The BET rate was found to be slowest in **6**–TiO_2 and fastest in **7**–TiO_2 on an early timescale. On laser excitation, electrons are injected from the MLCT state into the conduction band of TiO_2. Electrochemical studies suggest that phenol is a better donating group than tyrosine, which corroborates the decreased BET rate observed for **6** compared to **5**. However, the BET rate for **7** is the fastest due to the absence of electron-donating groups.

Experimental Section

Materials: Titanium(IV) tetraisopropoxide (97%), isopropyl alcohol, 4,4′-dimethyl-2,2′-bipyridine, *n*-butyllithium, 3,4-dimethoxybenzaldehyde, 2,2′-bipyridine, 4-methoxybenzaldehyde, 2-acetylpyridine, L-tyrosine ethyl ester hydrochloride and isopropyl alcohol were obtained from Sigma–Aldrich and used as received. Solvents such as THF, acetonitrile and isopropyl alcohol were dried and distilled prior to use. Nanopure water (Barnsted System, USA) was used in the preparation of aqueous solutions. All other reagents (AR grade) were procured from S.D. Fine Chemicals (India). HPLC grade acetonitrile (E. Merck, Mumbai, India) was used for all spectrophotometric titrations. Solvents were degassed thoroughly with IOLAR grade dinitrogen gas before use in the preparation of standard solutions.

Analytical Methods: FTIR spectra were recorded as KBr pellets in a cell fitted with a KBr window, using a Perkin–Elmer Spectra GX 2000 spectrometer. ^{1}H NMR spectra were recorded with a Bruker 200 MHz FT NMR (Avance-DPX 200) or Bruker 500 MHz FT NMR (Avance-DPX 500) using CD_3CN as the solvent and tetramethylsilane as an internal standard. ESI-MS measurements were carried out with a Waters QTof-Micro instrument. Microanalyses (C, H, N) were performed using a Perkin–Elmer 4100 elemental analyzer. Electronic spectra were recorded with a Shimadzu UV-3101 PC spectrophotometer; room temperature luminescence spectra were recorded with either a Fluorolog (Horiba Jobinyvon) or Perkin–Elmer LS 50B luminescence spectrofluorimeter, fitted with a red-sensitive photomultiplier tube. Electrochemical experiments were performed in acetonitrile with a CH-660A electrochemical instrument with a conventional three-electrode cell assembly and SCE as the reference electrode. All potentials have been corrected and quoted with respect to the Normal Hydrgen Electrode (NHE) in water.[78]

Femtosecond Visible Spectrometer: The femtosecond tunable visible spectrometer was developed based on a multi-pass amplified femtosecond Ti:Sapphire laser system from Avesta, Russia (1 kHz repetition rate at 800 nm, 50 fs, 800 μJ/pulse) as described previously.[79,80] The 800 nm output pulse from the multi-pass amplifier is split into two parts to generate pump and probe pulses. In this investigation we have used both the 800 nm (fundamental) and the frequency doubled 400 nm pulses as excitation sources. To generate pump pulses at 400 nm one part of 800 nm with 200 μJ/pulse is frequency doubled in BBO crystals. To generate visible probe pulses about 3 μJ of the 800 nm beam is focused onto a 1.5 mm thick sapphire window. The intensity of the 800 nm beam is adjusted by iris size and ND filters to obtain a stable white light continuum in the 400 to over 1000 nm region. The probe pulses are split into the signal and reference beams and are detected by two matched photodiodes with variable gain. We have kept the spot sizes of the pump beam and probe beam at the crossing point around 500 and 300 microns, respectively. The excitation energy density (at both 800 and 400 nm) was adjusted to ca. 2500 μJ/cm^2. The noise level of the white light is about about 0.5% with occasional spikes due to oscillator fluctuation. We have noticed that most laser noise is low-frequency noise and can be eliminated by comparing the adjacent probe laser pulses (pump blocked vs. unblocked using a mechanical chopper). The typical noise in the measured absorbance change is about $< 0.3\%$. The instrument response function for 400 nm excitation was obtained by fitting the rise time of the bleach of a sodium salt of *meso*-tetrakis(4-sulfonatophenyl)porphyrin at 710 nm and found to be 120 fs.

Preparation of Sample Solutions: The ruthenium complexes are insoluble in water and so sensitization was performed by dissolving the complexes in the smallest possible volume of acetonitrile (less than 2% of the total volume) and then adding the dissolved dye into the aqueous colloidal solution of the nanoparticles. The resulting solutions were stirred for half an hour and then kept in dark for 5 h for the dye to covalently bind to TiO_2. For all the measurements the sample solutions were degassed by continuously bubbling high purity nitrogen through the solutions.

Synthesis of TiO_2 Nanoparticles: TiO_2 nanoparticles were prepared by controlled hydrolysis of titanium(IV) tetraisopropoxide.[60,81] A solution of $Ti[OCH(CH_3)_2]_4$ (5 mL, Aldrich, 97%) in isopropyl alcohol (95 mL) was added dropwise (1 mL/min) to nanopure water (900 mL) at 2 °C at pH 1.5 (adjusted with HNO_3). The solution was continuously stirred for 10–12 h until the formation of a transparent colloid. The colloidal solution was concentrated at 35–40 °C with a rotary evaporator and dried with a nitrogen stream to yield a white powder. In this work, all colloidal samples have been prepared after dispersing the dry TiO_2 nanoparticles in water (20 g/L).

Syntheses

4′-Methyl-2,2′-bipyridinyl-4-carboxylic Acid (1): Compound **1** was prepared according to an adaptation of a reported procedure.[82] 4,4′-Dimethyl-2,2′-bipyridine (3 g, 16.3 mmol) and SeO_2 (2.2 g, 19.8 mmol) were dissolved in 1,4-dioxane (120 mL) and heated to reflux for 30 h with continuous stirring. The solution was filtered hot through celite. The filtrate was evaporated to dryness and was suspended in ethanol. To this suspension was added aq. $AgNO_3$ (3.04 g, 17.9 mmol) and a colour change to reddish yellow was observed. The suspension was stirred rapidly and NaOH solution (75 mL, 1 M) was added dropwise over half an hour. The reaction mixture was stirred for 24 h. Ethanol was removed by evaporation and the residue was collected by filtration in a grade 4 sintered glass crucible and washed with dilute aqueous NaOH and water. The filtrate was extracted into dichloromethane, and the pH of the aqueous layer was adjusted to 3.5 by addition of 6 N hydrochloric acid to precipitate a white solid. The solution along with the precipitate was kept in refrigerator for 6 h and then collected by filtration and dried. Pure **1** was obtained after continuously extracting this solid with acetone in a Soxhlet apparatus for seven days; yield 2.69 g, 77%. ESI-MS (*m*/*z*): calculated for $C_{12}H_{10}N_2O_2$ 214.22; found 215.15 [M + H$^+$]. ^{1}H NMR (500 MHz, [D$_6$]DMSO): δ = 8.87 [d, J = 4.5 Hz, 1 H, H^6 (bpy)]; 8.82 [s, 1 H, H^3 (bpy)]; 8.58 [d, J = 4.5 Hz, 1 H, H$^{6'}$ (bpy)]; 8.27 [s, 1 H, H$^{3'}$ (bpy)]; 7.87 [d, J = 4.5 Hz, 1 H, H^5 (bpy)]; 7.34 [d, J = 4 Hz, 1 H, H$^{5'}$ (bpy)]; 2.44 (s, 3 H, CH_3) ppm. IR (KBr): $\tilde{\nu}$ = 3427 (OH), 1710 (C=O) cm^{-1}. $C_{12}H_{12}N_2O_2$ (216.24): calcd. C 67.28, H 4.71, N 13.08; found C 67.0, H 4.97, N 13.1.

Ethyl-3-(4-hydroxyphenyl)-2-[(4′-methyl-2,2′-bipyridinyl-4-carbonyl)-amino]propionate (2): Synthesis of **2** was performed following a

modification of a literature procedure.[71] Compound **1** (500 mg, 2.336 mmol) was added to thionyl chloride (25 mL) and the solution was heated to reflux for 6 h. Excess thionyl chloride was removed by downward distillation and then under reduced pressure. To a solution of L-tyrosine ethyl ester hydrochloride (636.7 mg, 2.562 mmol) in dry distilled acetonitrile (30 mL) was added dry triethylamine (1 mL) and the acid chloride dissolved in dry acetonitrile dropwise over one hour. The solution was stirred for half an hour at room temperature and then heated to reflux for 12 h under dinitrogen. The solution was then cooled and filtered. The filtrate was evaporated to dryness, and the residue was dissolved in dichloromethane (≈ 30 mL) and washed three times with water to remove excess triethylamine. The organic phase was dried with anhydrous sodium sulfate and the solvents evaporated to dryness. The crude product was purified by chromatography using silica as the stationary phase and ethyl acetate/hexane as the eluent; yield 476.35 mg, 50%. ESI-MS (*m*/*z*): calculated for $C_{23}H_{23}N_3O_4$ 405.45; found 406.38 [M + H$^+$]. ^{1}H NMR (200 MHz, $CDCl_3$): δ = 8.71 [d, J = 5 Hz, 1 H, H^6 (bpy)]; 8.55 [s, 1 H, H^3 (bpy)]; 8.48 [d, J = 4.8 Hz, 1 H, $H^{6'}$ (bpy)]; 8.12 [s, 1 H, $H^{3'}$ (bpy)]; 7.64 [d, J = 4.8 Hz, 1 H, H^5 (bpy)]; 7.25 [d, J = 4.2 Hz, 1 H, $H^{5'}$ (bpy)]; 7.1 [d, J = 8.4 Hz, 2 H, H^3 (phenyl) and H^5 (phenyl)]; 6.72 [d, J = 8.2 Hz, 2 H, H^2 (phenyl) and H^6 (phenyl)]; 4.86–4.78 [m, 1 H, CH(COOEt)]; 4.18 (q, J = 7.2 Hz, 2 H, COOCH_2CH$_3$); 3.26–2.98 (m, 2 H, CH$_2$–ph); 2.43 (s, 3 H, bpy–CH$_3$); 1.23 (t, J = 7.2 Hz, 3 H, COOCH$_2$CH_3) ppm. IR (KBr): $\tilde{\nu}$ = 3320 (OH), 1728 (C=O)$_{ester}$, 1656 (C=O)$_{amide}$ cm^{-1}. $C_{23}H_{23}N_3O_4$ (405.45): calcd. C 68.13, H 5.72, N 10.36; found C 68.1, H 5.8, N 10.5.

4-(2,2′-Bipyridinyl-4-yl)phenol (3): Compound **3** was prepared following a reported procedure.[83] ESI-MS (*m*/*z*): calculated for $C_{16}H_{12}N_2O$ 248.28, found 249.16 [M + H$^+$], 271.15 [M + Na]$^+$. ^{1}H NMR (200 MHz, [D$_6$]DMSO): δ = 9.91 [s, 1 H, H (hydroxy)]; 8.73 [m, 1 H, $H^{6'}$ (bpy)]; 8.68 [d, J = 5.2 Hz, 1 H, H^6 (bpy)]; 8.62 [d, J = 1.2 Hz, 1 H, H^3 (bpy)]; 8.44 [d, J = 7.8 Hz, 1 H, $H^{3'}$ (bpy)]; 7.98 [td, J = 7.7 and 2 Hz, 1 H, $H^{4'}$ (bpy)]; 7.73–7.70 [m, 3 H, H^5 (bpy), H^2 (phenyl) and H^6 (phenyl)]; 7.53–7.46 [m, 1 H, $H^{5'}$ (bpy)]; 6.94 [d, J = 8.6 Hz, 2 H, H^3 (phenyl) and H^5 (phenyl)] ppm. IR (KBr): $\tilde{\nu}$ = 3397 (OH) cm^{-1}. $C_{16}H_{12}N_2O$ (248.28): calcd. C 77.40, H 4.87, N 11.28; found C 77.2, H 5.0, N 11.5.

4-[2-(4′-Methyl-[2,2′]bipyridinyl-4-yl)vinyl]benzene-1,2-diol (4): Compound **4** was prepared following a literature procedure.[84] ESI-MS (*m*/*z*): calculated for $C_{19}H_{16}N_2O_2$ 304.34, found 305.22 [M + H$^+$]. ^{1}H NMR (500 MHz, CD_3OD): δ = 8.54 [d, J = 5.5 Hz, 1 H, $H^{6'}$ (bpy)]; 8.52 [d, J = 5 Hz, 1 H, H^6 (bpy)]; 8.34 [s, 1 H, $H^{3'}$ (bpy)]; 8.13 [s, 1 H, H^3 (bpy)]; 7.53 [dd, J = 4, 1 Hz, 1 H, $H^{5'}$ (bpy)]; 7.43 [d, J = 16 Hz, 1 H, H (ethenyl)]; 7.32 [dd, J = 4, 1 Hz, 1 H, H^5 (bpy)]; 7.11 [d, J = 1.5 Hz, 1 H, H^2 (phenyl)]; 7.02–6.98 [m, 2 H, H (ethenyl) and H^6 (phenyl)]; 6.79 [d, J = 8 Hz, 1 H, H^5 (phenyl)]; 2.49 (s, 3 H, bpy-CH$_3$) ppm. IR (KBr): $\tilde{\nu}$ = 3238 (OH), 1590 (C=C) cm^{-1}. $C_{19}H_{16}N_2O_2$ (304.35): calcd. C 74.98, H 5.30, N 9.20; found C 74.5, H 5.3, N 9.7.

Ruthenium(II) Complex 5: $RuCl_3 \cdot xH_2O$ (51.2 mg, 0.247 mmol) and 2,2′-bipyridine (39 mg, 0.247 mmol) were dissolved in dimethylformamide (30 mL) and heated to 80 °C for 4 h. To the resulting solution was added **2** (100 mg, 0.247 mmol) and the reaction mixture was heated to 110 °C for 4 h. After 4 h, **4** (75.1 mg, 0.247 mmol) was added and the reaction mixture was heated to 135 °C for 8 h. The reaction mixture was allowed to cool to room temperature before the solvent was evaporated. The residue was dissolved in acetonitrile and was stirred with ten equiv. potassium hexafluorophosphate for 24 h. Acetonitrile was evaporated and the residue obtained was washed repeatedly with large volumes of water to remove the excess KPF_6. The crude product was purified by column chromatography by using silica as the stationary phase and acetonitrile/water/saturated aqueous KPF_6 as the eluent. The first fraction was collected and the solvents evaporated to dryness. It was redissolved in dichloromethane and two drops of acetonitrile and solvent extraction was repeated to remove the excess KPF_6 used in the eluent. The organic phase was dried with anhydrous sodium sulfate and evaporated to dryness to give the desired product. The compound was further purified by the vapour diffusion method of recrystallization (acetonitrile/diethyl ether). Although single crystals were not obtained, pure **5** was deposited; yield 85 mg, 27.4%. ESI-MS (*m*/*z*): calculated for $C_{52}H_{47}N_7O_6Ru$, [M – 2PF_6^-] 967.04; found 966.3 [M – 2PF_6^- – H$^+$]. ^{1}H NMR (200 MHz, CD_3CN): δ = 8.68 [s, 1 H, H^6 (bpy–tyr)]; 8.49 [d, J = 8.2 Hz, 5 H, H^6 and $H^{6'}$ (bpy), H^6 and $H^{6'}$ (bpy–cat), $H^{6'}$ (bpy–tyr)]; 8.05 [m, 3 H, H^3 and $H^{3'}$ (bpy), H^3 (bpy–tyr)]; 7.81 [m, 2 H, $H^{3'}$ (bpy–tyr), $H^{3'}$ (bpy–cat)]; 7.73–7.71 [m, 3 H, H^4 and $H^{4'}$ (bpy), H^3 (bpy–cat)]; 7.62–7.54 [m, 4 H, H (ethenyl), H^5 (bpy–tyr), H^5 and $H^{5'}$ (bpy)]; 7.4 [s, 3 H, $H^{5'}$ (bpy–tyr), $H^{5'}$ (bpy–cat), H^6 (catechol)]; 7.28–7.25 [m, 2 H, H^2 and H^5 (catechol)]; 7.15–7.04 [m, 4 H, H (ethenyl), H^5 (bpy–cat), H^2 and H^6 (phenol)]; 6.82 [d, J = 6.8 Hz, 2 H, H^3 and H^5 (phenol)]; 4.85–4.74 [m, 1 H, CH(COOEt)]; 4.15 (q, J = 7 Hz, 2 H, COOCH_2CH$_3$); 3.17–3.03 (m, 2 H, CH$_2$–phenol); 2.56 [s, 6 H, CH$_3$ (bpy–tyr), CH$_3$ (bpy–cat)]; 1.12 (t, J = 7.2 Hz, 3 H, COOCH$_2$CH_3) ppm. IR (KBr): $\tilde{\nu}$ = 3419 (OH), 1734 (C=O)$_{ester}$, 1605 (C=C), 841 (PF_6^-) cm^{-1}. $C_{52}H_{47}F_6N_7O_6PRu$ (1112.02): calcd. C 56.16, H 4.26, N 8.82; found C 55.9, H 4.3, N 8.6.

Ruthenium(II) Complex 6: Compound **6** was synthesized in an analogous manner to that of **5**. $RuCl_3 \cdot xH_2O$ (51.2 mg, 0.247 mmol) and 2,2′-bipyridine (39 mg, 0.247 mmol) were dissolved in dimethylformamide (30 mL) and heated to 80 °C for 4 h. To the resulting solution was added **3** (61.5 mg, 0.247 mmol) and the reaction mixture was heated to 110 °C for 5 h. The reaction mixture was allowed to stand for 4 h before the addition of **4** (75.1 mg, 0.247 mmol) and the reaction mixture was heated to 140 °C for 15 h. The purification steps are the same as described above for **5**; yield 90 mg, 33%. ESI-MS (*m*/*z*): calculated for $C_{45}H_{36}N_6O_3Ru$, [M – 2PF_6^-] 809.88, found 808.24 [M – 2PF_6^- – H$^+$]. ^{1}H NMR (200 MHz, CD_3CN): δ = 8.70 [s, 4 H, H^3, H^6 and $H^{6'}$ (bpy–ph), H^6 or $H^{6'}$ (bpy)]; 8.53 [d, J = 7.4 Hz, 4 H, H^6 and $H^{6'}$ (bpy–cat), H^6 or $H^{6'}$ (bpy), H^5 or $H^{5'}$ (bpy)]; 8.39 [d, J = 7.6 Hz, 1 H, $H^{3'}$ (bpy–ph)]; 8.12–8.04 [m, 5 H, H^3 and $H^{3'}$ (bpy), H^3 and $H^{3'}$ (bpy–cat), $H^{4'}$ (bpy–ph)]; 7.88 [d, J = 6 Hz, 2 H, H^4 and $H^{4'}$ (bpy)]; 7.83–7.74 [m, 5 H, H^2 and H^6 (phenol), H^5 (bpy–ph), H^5 (bpy–cat), H^5 or $H^{5'}$ (bpy)]; 7.62 [m, 2 H, H^6 (catechol), H^5 (bpy–cat)]; 7.45–7.39 [m, 3 H, H (ethenyl), H^2 and H^5 (catechol)]; 7.28 [t, J = 6.4 Hz, 1 H, $H^{5'}$ (bpy–ph)]; 7.02 [m, 3 H, H (ethenyl), H^3 and H^5 (phenol)]; 2.55 [s, 3 H, CH$_3$ (bpy–cat)] ppm. IR (KBr): $\tilde{\nu}$ = 3438 (OH), 1606 (C=C), 840 (PF_6^-) cm^{-1}. $C_{45}H_{36}F_6N_6O_3PRu$ (954.85): calcd. C 56.6, H 3.8, N 8.8; found C 56.2, H 4.1, N 9.0.

Acknowledgments

The Board of Research in Nuclear Sciences (Department of Atomic Energy, Government of India) and the Council of Scientific and Industrial Research (CSIR) (India) have supported this work. T. B. acknowledges BRNS for a Research Fellowship. We thank Dr. P. K. Ghosh (CSMCRI), Dr. S. K. Sarkar (BARC) and Dr. T. Mukherjee (BARC) for their interest in this work.

[1] M. Pelizzetti, M. Schiavello, in: *Photochemical Conversion and Storage of Solar Energy*, Kluwer, Dordrecht, **1997**.

[2] B. O'Regan, M. Grätzel, *Nature* **1991**, *353*, 737–740.
[3] Y. Bai, Y. Cao, J. Zhang, M. Wang, R. Li, P. Wang, S. M. Zakeeruddin, M. Grätzel, *Nat. Mater.* **2008**, *7*, 626–630.
[4] K. Kalyansundaram, M. Gratzel, *Coord. Chem. Rev.* **1998**, *77*, 347–414.
[5] E. Ghadiri, N. Taghavinia, S. M. Zakeeruddin, M. Grätzel, J.-E. Moser, *Nano Lett.* **2010**, *10*, 1632–1638.
[6] K. Lee, S. Park, M. J. Ko, K. Kim, N.-G. Park, *Nat. Mater.* **2009**, *8*, 665–671.
[7] F. Gao, Y. Wang, D. Shi, J. Zhang, M. Wang, X. Jing, R. Humphry-Baker, P. Wang, S. M. Zakeeruddin, M. Grätzel, *J. Am. Chem. Soc.* **2008**, *130*, 10720–10728.
[8] J. E. Moser, *Nat. Mater.* **2005**, *4*, 723–724.
[9] P. Wang, S. M. Zakeeruddin, R. Humphry-Baker, J.-E. Moser, M. Grätzel, *Adv. Mater.* **2003**, *15*, 2101–2104.
[10] U. Bach, D. Lupo, P. Comte, J. E. Moser, F. Weissörtel, J. Salbeck, H. Spreitzer, M. Grätzel, *Nature* **1998**, *395*, 583–585.
[11] A. Reynal, A. Forneli, E. Martinez-Ferrero, A. Sanchez-Diaz, A. Vidal-Ferran, B. C. O'Regan, E. Palomares, *J. Am. Chem. Soc.* **2008**, *130*, 13558–13567.
[12] S. Atobello, R. Argazzi, S. Caramori, C. Contado, S. Da Fre, P. Rubino, C. Chone, G. Larramona, C. A. Bignozzi, *J. Am. Chem. Soc.* **2005**, *127*, 15342–15343.
[13] M. K. Nazeeruddin, P. Pechy, T. Renouard, S. M. Zakeeruddin, R. Humphry-Baker, P. Comte, P. Liska, L. Cevey, E. Costa, V. Shklover, L. Spiccia, G. B. Deacon, C. A. Bignozzi, M. Gratzel, *J. Am. Chem. Soc.* **2001**, *123*, 1613–1624.
[14] P. Wang, R. Humphry-Baker, J. E. Moser, S. M. Zakeeruddin, M. Gratzel, *Chem. Mater.* **2004**, *16*, 3246–3251.
[15] N. Robertson, *Angew. Chem.* **2006**, *118*, 2398; *Angew. Chem. Int. Ed.* **2006**, *45*, 2338–2345.
[16] C. Lee, J.-H. Yum, H. Choi, S. O. Kang, J. Ko, R. Humphrey-Baker, M. Gratzel, M. K. Nazeeruddin, *Inorg. Chem.* **2008**, *47*, 2267–2273.
[17] Y. Tachibana, J. E. Moser, M. Gratzel, D. R. Klug, J. R. Durrant, *J. Phys. Chem.* **1996**, *100*, 20056–20062.
[18] H. Choi, C. Baik, S. Kim, M. S. Kang, X. Xu, H. S. Kang, S. O. Kang, J. Ko, M. K. Nazeeruddin, M. Gratzel, *New J. Chem.* **2008**, *32*, 2233–2237.
[19] R. Argazzi, C. A. Bignozzi, *J. Am. Chem. Soc.* **1995**, *117*, 11815–11816.
[20] R. Agrazzi, C. A. Bignozzi, T. A. Heimer, F. N. Castellano, G. M. Meyer, *J. Phys. Chem. B* **1997**, *101*, 2591–2597.
[21] P. Bonhote, J. E. Moser, N. Vlachopoulos, L. Walder, S. M. Zakeeruddin, R. Humphrey-Baker, P. Pechy, M. Gratzel, *Chem. Commun.* **1996**, 1163–1164.
[22] P. Bonhote, J. E. Moser, R. Humphrey-Baker, N. Vlachopoulos, S. M. Zakeeruddin, L. Walder, M. Gratzel, *J. Am. Chem. Soc.* **1999**, *121*, 1324–1336.
[23] S. Handa, H. Wietasch, M. Thelakkat, J. R. Durrant, S. A. Haque, *Chem. Commun.* **2007**, 1725–1727.
[24] C. S. Karthikeyan, H. Wietasch, M. Thelakkat, *Adv. Mater.* **2007**, *19*, 1091–1095.
[25] N. Hirata, J. J. Lagref, E. J. Palomares, J. R. Durrant, M. K. Nazeeruddin, M. Gratzel, D. D. Censo, *Chem. Eur. J.* **2004**, *10*, 595–602.
[26] H. J. Snaith, C. S. Karthikeyan, A. Petrozza, J. Teuscher, J. E. Moser, M. K. Nazeeruddin, M. Thelakkat, M. Gratzel, *J. Phys. Chem. C* **2008**, *112*, 7562–7566.
[27] S. A. Haque, S. Handa, K. Peter, E. Palomares, M. Thelakkat, J. R. Durrant, *Angew. Chem.* **2005**, *117*, 5886; *Angew. Chem. Int. Ed.* **2005**, *44*, 5740–5744.
[28] K. Willinger, K. Fischer, R. Kisselev, M. Thelakkat, *J. Mater. Chem.* **2009**, *19*, 5364–5376.
[29] J. Y. Li, C. Y. Chen, J. G. Chen, C. J. Tan, K. M. Lee, S. J. Wu, Y. L. Tung, H. H. Tsai, K. C. Ho, C. G. Wu, *J. Mater. Chem.* **2010**, *20*, 7158–7164.
[30] H. Wolpher, S. Sinha, J. Pan, A. Johansson, M. J. Lundqvist, P. Persson, R. Lomoth, J. Bergquist, L. Sun, V. Sundstrom, B. Akermark, T. Polivka, *Inorg. Chem.* **2007**, *46*, 638–651.
[31] J. Pan, Y. Xu, G. Benko, Y. Feyziyev, S. Styring, L. Sun, B. Akermark, T. Polivka, V. Sundstrom, *J. Phys. Chem. B* **2004**, *108*, 12904–12910.
[32] M. K. Nazeeruddin, S. M. Zakeeruddin, R. Humphrey-Baker, M. Jirousek, P. Liska, N. Vlachopoulos, V. Skhlover, C. H. Fischer, M. Gratzel, *Inorg. Chem.* **1999**, *38*, 6298–6305.
[33] C. R. Rice, M. D. Ward, M. K. Nazeeruddin, M. Gratzel, *New J. Chem.* **2000**, *24*, 651–652.
[34] C. She, J. Guo, S. Irle, K. Morokuma, D. L. Mohler, H. Zabri, F. Odobel, K. T. Youm, F. Liu, J. T. Hupp, T. Lian, *J. Phys. Chem. A* **2007**, *111*, 6832–6842.
[35] P. Kar, S. Verma, A. Das, H. N. Ghosh, *J. Phys. Chem. C* **2009**, *113*, 7970–7977.
[36] P. Kar, S. Verma, A. Sen, A. Das, H. N. Ghosh, *Inorg. Chem.* **2010**, *49*, 4167–4174.
[37] G. Ramakrishna, D. A. Jose, D. Krishna Kumar, A. Das, D. K. Palit, H. N. Ghosh, *J. Phys. Chem. B* **2005**, *109*, 15445–15453.
[38] G. D. Fasman, in: *Handbook of Biochemistry and Molecular Biology, Proteins, I*, CRC Press, **1976**.
[39] I. B. Berlman, in: *Handbook of Fluorescence Spectra of Aromatic Molecules*, Academic Press, **1971**.
[40] D. A. Jose, P. Kar, D. Koley, B. Ganguly, W. Thiel, H. N. Ghosh, A. Das, *Inorg. Chem.* **2007**, *46*, 5576–5584.
[41] K. Kalyanasundaram, in: *Photochemistry of Polypyridine and Porphyrin Complexes*, Academic Press, London, **1992**, chapter 6.
[42] C. Tommos, J. J. Skalicky, D. L. Pilloud, J. Wand, P. L. Dutton, *Biochemistry* **1999**, *38*, 9495–9507.
[43] S = Sensitizer and therefore denotes **5** or **6**.
[44] D. Kuang, B. Wenger, C. Klein, J. E. Moser, R. H. Baker, S. M. Zakeeruddin, M. Gratzel, *J. Am. Chem. Soc.* **2006**, *128*, 4146–4154.
[45] S. Verma, P. Kar, A. Das, D. K. Palit, H. N. Ghosh, *J. Phys. Chem. C* **2008**, *112*, 2918–2926.
[46] S. Verma, P. Kar, A. Das, D. K. Palit, H. N. Ghosh, *Chem. Eur. J.* **2010**, *16*, 611–619.
[47] J. Moser, S. Punchihewa, P. P. Infelta, M. Gratzel, *Langmuir* **1991**, *7*, 3012–3018.
[48] T. Rajh, L. X. Chen, K. Lukas, T. Liu, M. C. Thurnauer, D. M. Teide, *J. Phys. Chem. B* **2002**, *106*, 10543–10552.
[49] G. Ramakrishna, A. K. Singh, D. K. Palit, H. N. Ghosh, *J. Phys. Chem. B* **2004**, *108*, 1701–1707.
[50] S. Kaniyankandy, S. Verma, J. A. Mondal, D. K. Palit, H. N. Ghosh, *J. Phys. Chem. C* **2009**, *113*, 3593–3599.
[51] G. Ramakrishna, H. N. Ghosh, A. K. Singh, D. K. Palit, J. P. Mittal, *J. Phys. Chem. B* **2001**, *105*, 12786–12796.
[52] a) G. Ramakrishna, S. Verma, D. A. Jose, D. Krishna Kumar, A. Das, D. K. Palit, H. N. Ghosh, *J. Phys. Chem. B* **2006**, *110*, 9012–9021; b) S. Verma, A. Ghosh, A. Das, H. N. Ghosh, *Chem. Eur. J.* **2011**, *17*, 3458; c) S. Verma, P. Kar, A. Das, H. N. Ghosh, *Chem. Eur. J.* **2011**, *17*, 1561.
[53] A. Cannizo, F. V. Mourik, W. Gawelda, G. Zgrablic, C. Bressler, M. Chergui, *Angew. Chem.* **2006**, *118*, 3246; *Angew. Chem. Int. Ed.* **2006**, *45*, 3174–3176.
[54] D. Kuciauskas, J. E. Monat, R. Villahermosa, H. B. Gray, N. S. Lewis, J. K. McCusker, *J. Phys. Chem. B* **2002**, *106*, 9347–9358.
[55] J. McCusker, *Acc. Chem. Res.* **2003**, *36*, 876–887.
[56] W. Henry, C. G. Coates, C. Brady, K. L. Ronayne, P. Matousek, M. Towrie, S. W. Botchway, A. W. Parker, J. G. Vos, W. R. Browne, J. J. McGarvey, *J. Phys. Chem. A* **2008**, *112*, 4537–4544.
[57] A. Vlcek Jr, *Coord. Chem. Rev.* **2000**, *200*, 933–978.
[58] J. Z. Zhang, *Acc. Chem. Res.* **1997**, *30*, 423–429.
[59] D. P. Colombo Jr, R. M. Bowman, *J. Phys. Chem.* **1996**, *100*, 18445–18449.
[60] H. N. Ghosh, *J. Phys. Chem. B* **1999**, *103*, 10382–10387.
[61] T. Hannapel, B. Burfeindt, W. Storck, F. Willig, *J. Phys. Chem. B* **1997**, *101*, 6799–6802.
[62] J. B. Asbury, E. Hao, Y. Q. Wang, H. N. Ghosh, T. Lian, *J. Phys. Chem. B* **2001**, *105*, 4545–4557.

[63] J. B. Asbury, R. J. Ellingson, H. N. Ghosh, S. Ferrere, A. Nozik, T. Lian, *J. Phys. Chem. B* **1999**, *103*, 3110–3119.
[64] G. Benko, J. Kallioinen, J. E. I. Korppi-Tommola, A. Yartsev, V. Sundstrom, *J. Am. Chem. Soc.* **2002**, *124*, 489–493.
[65] R. J. D. Miller, G. L. McLendon, A. J. Nozik, W. Schmickler, F. Willig, in *Surface Electron Transfer Processes*, VCH Publisher, Inc., Chapter 5.
[66] C. She, J. Guo, T. Lian, *J. Phys. Chem. B* **2007**, *111*, 6903–6912.
[67] T. A. Heimer, S. T. D'Arcangelis, F. Farzad, J. M. Stipkala, G. J. Meyer, *Inorg. Chem.* **1996**, *35*, 5319–5324.
[68] J. B. Asbury, E. Hao, Y. Wang, T. Lian, *J. Phys. Chem. B* **2000**, *104*, 11957–11964.
[69] J. He, G. Benko, F. Korodi, T. Polivka, R. Lomoth, B. Akermark, L. Sun, A. Hagfeldt, V. Sundstrom, *J. Am. Chem. Soc.* **2002**, *124*, 4922–4932.
[70] C. Kleverlaan, M. Alebbi, R. Agrazzi, C. A. Bignozzi, G. M. Hasselman, G. J. Meyer, *Inorg. Chem.* **2000**, *39*, 1342–1343.
[71] R. Ghanem, Y. Xu, J. Pan, T. Hoffmann, J. Andersson, T. Polivka, T. Pascher, S. Styring, L. Sun, V. Sundstrom, *Inorg. Chem.* **2002**, *41*, 6258–6266.
[72] M. Sjodin, S. Styring, H. Wolpher, Y. Xu, L. Sun, L. Hammarström, *J. Am. Chem. Soc.* **2005**, *127*, 3855–3863.
[73] R. A. Marcus, N. Sutin, *Biochim. Biophys. Acta* **1985**, *811*, 265–322.
[74] A. Hagfeldt, M. Gratzel, *Chem. Rev.* **1995**, *95*, 49–68.
[75] H. Lu, J. N. Prieskorn, J. T. Hupp, *J. Am. Chem. Soc.* **1993**, *115*, 4927–4928.
[76] X. Dang, J. T. Hupp, *J. Am. Chem. Soc.* **1999**, *121*, 8399–8400.
[77] G. Ramakrishna, H. N. Ghosh, *J. Phys. Chem. B* **2001**, *105*, 7000–7008.
[78] M. K. Nazeeruddin, S. M. Zakeeruddin, K. Kalyanasundaram, *J. Phys. Chem.* **1993**, *97*, 9607–9612.
[79] G. Ramakrishna, A. K. Singh, D. K. Palit, H. N. Ghosh, *J. Phys. Chem. B* **2004**, *108*, 4775–4783.
[80] G. Ramakrishna, A. K. Singh, D. K. Palit, H. N. Ghosh, *J. Phys. Chem. B* **2004**, *108*, 12489–12496.
[81] D. Bahnemann, A. Henglein, J. Lilie, L. Spanhel, *J. Phys. Chem.* **1984**, *88*, 709–711.
[82] D. G. McCafferty, B. M. Bishop, C. G. Wall, S. G. Hughes, S. L. Mecklenberg, T. J. Meyer, B. W. Erickson, *Tetrahedron* **1995**, *51*, 1093–1106.
[83] M. A. Hayes, C. Meckel, E. Schatz, M. D. Ward, *J. Chem. Soc., Dalton Trans.* **1992**, 703–708.
[84] A. D. Shukla, B. Whittle, H. C. Bajaj, A. Das, M. D. Ward, *Inorg. Chim. Acta* **1999**, *285*, 89–96.

Received: April 15, 2011
Published Online: August 17, 2011

